Authors accepted manuscript.
Article published in IEEE Transactions on Microwave Theory and Techniques (Vol. 69, Issue 3, March 2021)
The final published version available at https://doi.org/10.1109/TMTT.2020.3048149


# A Novel Design Technique for mm-Wave Mismatch Terminations

Mahmoud Elsaadany, *Member, IEEE*, Mohamed Mamdouh. M. Ali, *Student Member, IEEE*, Shoukry I. Shams, *Member, IEEE*, Tayeb A. Denidni, *Member, IEEE*, and Ghyslain Gagnon *Member, IEEE*

***Abstract*—The mismatch terminations are essential components in measurement setups of various active and passive microwave components. The main objective of such components is to provide a certain reflection level with a flat response over the operating bandwidth. The need for mm-wave mismatch terminations has increased due to the expansion o using mm-wave frequency ranges in future communication systems. The mm-wave bands are considered among the essential bands for the 5G communication system, which is expected to launch this year. In addition, the utilization of these bands is expected to increase in the 6G standard. In this article, we introduce a novel systematic procedure to design mismatch terminations. Moreover, two examples of mismatch terminations are designed with reflection levels of -9.5 dB and -12.7 dB, with the operating band is 32GHz-38GHz. For experimental validation, proposed design is fabricated and measured, where a good agreement is achieved between the simulated and the measured response.**

***Index Terms*—Mismatch Termination - mm-wave component - flat reflection**

## I. Introduction

MICROWAVE terminations are one-port networks that transform the electrical energy into heat. Terminations are classified as passive lossy component, and are deployed in measurement setups and protection systems. In general, a microwave termination consists of a housing filled with an absorptive material. The absorptive material should have a high loss tangent to provide high attenuation for the propagating signal. The absorptive material can be a lossy plastic such as carbon tetrachloride or a ceramic based material such as Silicon Carbide (SiC) [1], [2]. The housing design depends on the power handling of the unit with respect to the waveguide size. A load housing can be a simple cover or a cover attached to heat convection structure (fins). In some cases, this load cover is formed of a housing with a surrounding coolant chamber. For high power applications, the cooling process is performed using liquid flow, where the commonly used fluid is water due to its low cost and the unlimited supply [3], [4]. Microwave terminations, also referred to as dummy loads, are typically characterized by the deep matching level [5], [6] as well as the power handling capability [7], [8]. However, some sophisticated measurement setups require a certain reflection level to perform an accurate assessment of the Device Under Test (DUT) performance. In such cases, the DUT is terminated with a mismatch load that provide a specific reflection level with a flat response within the operating band.

To the contrary of the dummy loads, the matching level of the mismatch loads is defined within a certain range (e.g. -10 dB $\pm$ 0.5 dB), while the standard loads' matching level is specified below a certain limit (e.g. $\leq$-30 dB). These mismatch loads are used in the assessment of various components, especially microwave amplifiers [9], where it is significant to characterize the performance of amplifiers in terms of stability, and voltage breakdown. This can be carried out though evaluating the amplifier response while being subjected to different reflection levels. Hence, mismatch load is used to emulate the electrical loading effect during testing. The mismatch load is selected in a way such that it has a similar impedance of the actual device that will be connected in the RF system.

In an RF system, the mismatch load is typically used to emulate an antenna. By using this load instead of an actual antenna, the transceiver unit can be tested and configured without actually radiating waves into the surroundings. This way, high power radiating systems can be tested in an environmental-friendly scenario without the need of expensive outdoor setups [10], [11]. Another important application for the dummy loads is the decoupling of the antennas in antenna arrays, where most of these load types are implemented in printed technologies [12], [13].

Despite of their significant importance, the literature lacks the existence of a clear design methodology and configuration of mismatch terminations. In this article, a novel systematic procedure is proposed to design mismatch terminations with different reflection levels. An accurate model is presented to evaluate the reflection level, where the proposed model is validated through the comparison with the numerical simulations. In addition, an innovative configuration for the mismatch load is proposed to provide a specific reflection level, while ensuring a flat response within the operating bandwidth. Furthermore, the proposed design procedure takes into account real-life aspects such as the non-ideal absorptive

Mahmoud Elsaadany and Ghyslain Gagnon are with the Electrical Engineering Department, École de technologie supérieure (ETS), Montréal, Quebec, Canada. Mohamed Mamdouh M. Ali is with the Department of Electrical Engineering, Assiut University, Egypt. Shoukry I. Shams is with the Department of Electrical and Computer Engineering, Concordia University, Montréal, Quebec, Canada. Tayeb A. Denidni is with INRS-EMT, University of Quebec, Montréal, Quebec, Canada.

material characterization. Finally, the proposed procedure is validated through solving two mismatch loads design problems using analysis and simulations, and final design of a $-9.5$ dB mismatch load is fabricated and measured.

This article is organized as follows: In section II, the modeling and analysis of the basic building block of the proposed configuration are presented. Further, the capacitive post is analyzed, and is proposed to enhance the flatness of the final structure. In section III, the proposed configuration of the mismatch load is discussed in details, where this configuration is modeled as cascaded sections of single-ridge sections. Section III discusses the performance of the proposed design based on the assumption of ideal response of the absorptive material, where is discovered not to be an accurate assumption. The actual response of the absorptive material is presented and analyzed in Section IV, where the design procedure is modified to accommodate for the realistic response. Experimental validation of the proposed procedure through a fabricated prototype follows in Section V. Finally, the outcomes of this article are summarized in Section VI.

## II. Analytical Models

The proposed mismatch load design consists of a mismatch section connected to a high power brick load, as shown in Fig.1. The mismatch section is a rectangular waveguide loaded with posts with rectangular and circular cross-section. The rectangular posts are mainly used to achieve the required reflection, while the cylindrical posts are deployed to provide reflection balance within the operation bandwidth. The rectangular stub is modelled as single-ridge structure, where an accurate model for the discontinuity between the rectangular waveguide and single-ridge will be presented in this section. The model that will be proposed in this section is a modified version of the classical model used in the literature. However, the cylindrical post inside a rectangular waveguide can be modeled as an $LC$ circuit, where a good approximation for the resultant susceptance is deployed based on the classical approaches reported in the literature. Accordingly, in the coming part, a detailed description of the single ridge modified model will be illustrated. On the other hand, the cylindrical post model will be briefly discussed.

### A. Single-Ridge Post Model

In the proposed configuration of our design, a single-ridge section is deployed as a basic building block to cause the mismatch reflection. The first step is to develop an accurate model for the metallic single-ridge placed between two rectangular waveguide sections, as shown in Fig. 2(a). This structure can achieve the required value for the reflection with a variation around $\pm$ 1 dB , however, our target is to achieve a $\pm$ 0.1 dB over the operating bandwidth. This flat response will

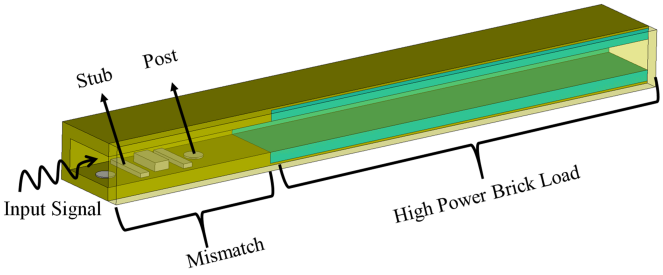


Fig. 1. The configuration of the proposed design of mismatch terminations.

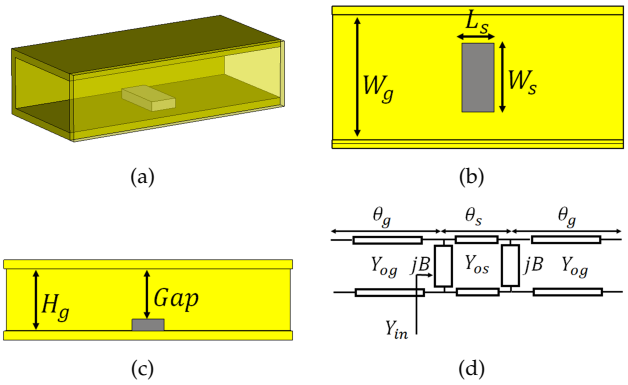


Fig. 2. The single ridge structure and circuit model. (a) 3D cross-section view. (b) Side cross-section view. (c) Top cross-section view. (d) Circuit model.

be achieved through three cascaded single ridge stages and two cylindrical posts as shown in Fig. 1. Figs. 2(b) and 2(c) show the geometrical configurations having all the parameter of the single-ridge placed inside a rectangular waveguide. Each single ridge structure can be fully defined by $L_s$, and the ratios $\frac{W_s}{W_g}$ and $\frac{H_{gap}}{H_g}$, where $W_g$ and $H_g$ are the cross-section dimensions of the rectangular waveguide, $W_s$, $H_{gap}$ and $L_s$, are the ridge width, ridge gap, and ridge length, respectively. The initial dimensions for the single ridge are obtained through an equivalent circuit representation of single ridge structure connected to a rectangular waveguide. The proposed equivalent circuit is based on transmission line model shown in Fig. 2(d), where $Y_{og} = \frac{1}{Z_{og}}$ and $Y_{os} = \frac{1}{Z_{os}}$ are the characteristic admittances of the rectangular waveguide and single ridge waveguide, respectively. The power-voltage definition for the characteristics impedance is used to calculate the impedance for both rectangular $Z_{og}$ and single ridge wave guides $Z_{os}$ [14]–[16]. Assuming a $TE_{10}$ propagating mode in the rectangular waveguide, the rectangular waveguide characteristics impedance $Z_{og}$ can be calculated as follow [14]:

$$Z_{og} = 240\pi\left(\frac{H_g}{W_g}\right)\frac{1}{\sqrt{1-\left(\frac{f_{cg}}{f}\right)^2}} \quad (1)$$

where, $f_{cg}$ is the cutoff frequency of the TE-mode for the rectangular waveguide and $f$ is the operating frequency.

$$-\cot\left(\frac{\pi}{2}\frac{f_{cs}}{f_{cg}}\left[1-\frac{W_s}{W_g}\right]\right)+\frac{H_g}{H_{gap}}\times\tan\left(\frac{\pi}{2}\frac{f_{cs}}{f_{cg}}\frac{W_s}{W_g}\right)-\frac{f_{cs}}{f_{cg}}\frac{H_g}{W_g}\times\ln\left[\sin^2\left(\frac{\pi}{2}\frac{H_{gap}}{H_g}\right)\right]=0 \quad (2)$$

While, the cutoff frequency of the single ridge structure $f_{cs}$ can be determined based on transverse resonance method by solving Eq. 2 (top of next page) , [18], [19]. Therefore, the single ridge waveguide characteristics impedance $Z_{os}$ can be calculated as follow [14]:

$$Z_{os} = \frac{Z_{os}(\infty)}{\sqrt{1-(\frac{f_{cs}}{f})^2}} \quad (3)$$

where, $Z_{os}(\infty)$ is the impedance at infinite frequency and is calculated using Eq. 4 (top of next page).

In addition, the discontinuity between the single ridge and rectangular waveguides is considered and represented by a susceptance $B$ as shown in Fig. 2(d). This susceptance can be calculated as follow [14]:

$$B = \frac{W_s W_{eff}}{60\ \pi\ H_{gap}\ \lambda_g}\ln\frac{1}{\sin\frac{\pi}{2}\frac{H_{gap}}{H_g}} \quad (6)$$

where, $\lambda_g$ is the guided wavelength in the rectangular waveguide and $W_{eff}$ is the effective width This discontinuity has been addressed before, while it has the full width of the guiding structure. Substituting with the physical ridge width does not represent the actual contribution of this discontinuity, specially that most of the field is concentrated at the center of the waveguide. A major modification is proposed here to utilize the previously derived capacitance formula. In this article, we replaced the physical width of the ridge by the effective width, where this effective width is proportional to the field concentration in the ridge region. The effective ridge width is calculated through evaluating the ratio between the field concentrated in the ridge region compared to the field within the entire rectangular waveguide. Assuming the incident $TE10$ mode with amplitude A is applied at the input port with electric field that can be written as [17]:

$$\vec{E} = A\ cos(\frac{\pi x}{a})\ \vec{a_y} \quad (7)$$

Therefore, the effective width can be given as:

$$W_{eff} = W_g\frac{2\mid\int_0^{W_s/2}Edx\mid}{2\mid\int_0^{W_g/2}Edx\mid} = W_g sin(\frac{\pi W_s}{W_g}) \quad (8)$$

Therefore, the input reflection coefficient $\Gamma$ is calculated as:

$$\Gamma = \frac{Y_{og}-Y_{in}}{Y_{og}+Y_{in}} \quad (9)$$

where,$Y_{in}$ is the circuit admittance as shown in Fig. 2(d).

To verify the proposed model, different values for both ridge gap $H_{gap}$ and ridge width $W_s$ in WR28 rectangular waveguide are considered, where the reflection coefficient $\Gamma$ at operating bandwidth is calculated and compared with CST simulation in Fig. 3.

### *B. Cylindrical Post model*

As will be discussed in more details in a later section, the metallic cylindrical post can add a localized susceptance, which will be deployed to get a flat response within a certain bandwidth. The rectangular waveguide loaded with a cylindrical post (shown in Fig. 4) was addressed in many articles and text books, where different models were provided and validated [20]–[22]. In this article, we used the model illustrated in [23], to calculate the susceptance of the cylindrical post inside the waveguide.

## III. Mismatch Load Configuration

In order to obtain a stable reflection over a wide frequency band, cascaded stages of single ridge structures are deployed. Fig. 5(a) shows a design with three cascaded stages, which will be used for illustration in the rest of this paper. The three ridges are symmetrically built around the central ridge section to minimize the number of design parameters as shown in Figs.5(b) and 5(c). In this section, we are going to deploy the previously described model to design two mismatch load examples with a reflection levels of -9.5 dB and -12.7 dB, while the objective mismatch loads have a zero phase at the band center.

The initial dimensions of the cascaded single ridge sections are calculated based on the approximate expression of the total reflection coefficient $\Gamma_t = 2\Gamma_2 + \Gamma_1$, where $\Gamma_1$ and $\Gamma_2$ are the reflection coefficients of the center and the terminal single ridge sections, respectively. To simplify the initial dimensions extraction process, the reflection level of the center section is assumed to be twice the reflection level of the terminal sections. Assuming the required reflection coefficient is -9.5 dB and $\Gamma_t = 4\Gamma_2 = 10^{-9.5/20}$, then $\Gamma_1$ = -15.5 dB and $\Gamma_2$= -21.54 dB are the required reflection coefficients for the center and the terminal single ridge sections. The initial dimensions of the single ridge section that achieved the required reflections $\Gamma_1$ and $\Gamma_2$ can be obtained through parametric sweep using the previously mentioned mathematical formulations, where the dimensions are $H_{Gap1}$= 0.123 in, $W_{s1}$= 0.15 in, $H_{Gap2}$=0.1309 in, $W_{s2}$=0.2 in. These initial dimensions are deployed as a starting point, where further optimization is performed to obtain the required reflection level for the entire structure based on the

$$Z_{os}(\infty) = \frac{120\pi \frac{\pi}{2}\frac{H_g}{W_g}\frac{H_{gap}}{H_g}\frac{f_{cs}}{f_{cg}}}{\frac{\pi}{4}\frac{W_s}{W_g}\frac{f_{cs}}{f_{cg}} + \frac{1}{4}\sin\left(\pi\frac{W_s}{W_g}\frac{f_{cs}}{f_{cg}}\right) - \frac{H_{gap}}{H_g}\frac{H_g}{W_g}\frac{f_{cs}}{f_{cg}}\cos^2\left(\frac{\pi}{2}\frac{W_s}{W_g}\frac{f_{cs}}{f_{cg}}\right)\ln\left[\sin^2\left(\frac{\pi}{2}\frac{H_{gap}}{H_g}\right)\right] + Y} \quad (4)$$

where

$$Y = \frac{1}{4}\frac{H_{gap}}{H_g}\frac{\cos^2\left(\frac{\pi}{2}\frac{W_s}{W_g}\frac{f_{cs}}{f_{cg}}\right)}{\sin^2\left(\frac{\pi}{2}\frac{f_{cs}}{f_{cg}}\left[1-\frac{W_s}{W_g}\right]\right)}\left[\pi\frac{f_{cs}}{f_{cg}}\left[1-\frac{W_s}{W_g}\right] - \sin\left(\pi\frac{f_{cs}}{f_{cg}}\left[1-\frac{W_s}{W_g}\right]\right)\right] \quad (5)$$

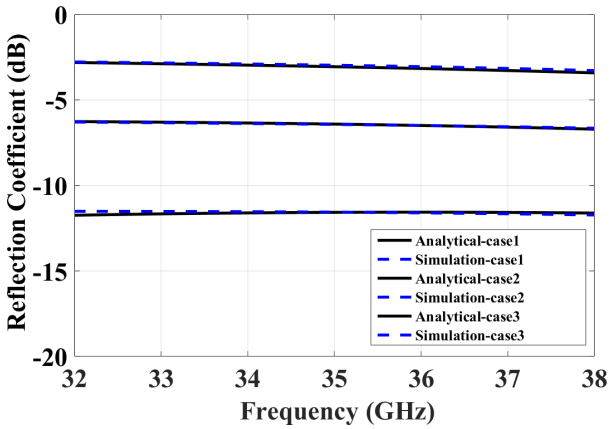


Fig. 3. Reflection coefficient for one stage of the single-ridge structure.

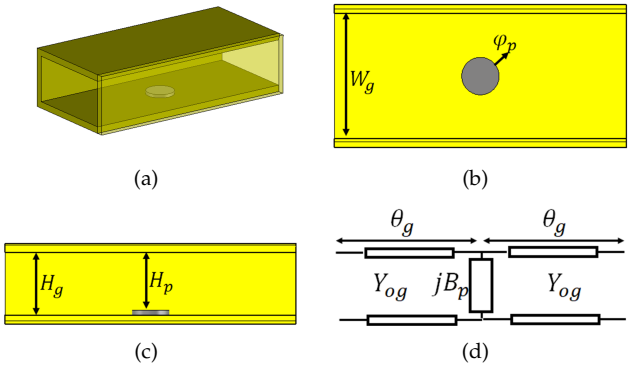


Fig. 4. The cylindrical post and circuit model. (a) 3D cross-section view. (b) Side cross-section view. (c) Top cross-section view. (d) Circuit model.

accurate circuit model shown in Fig. 6. Two examples of reflection coefficients -9.5 dB (Design I) and -12.7 dB (Design II) are studied, where the optimum dimensions of the cascaded single-ridge structures shown in Fig. 5 are listed in Table I.

Fig. 7 shows the calculated reflection coefficient through the circuit model compared with the CST simulation results, where a good agreement can be observed. To improve the flatness of the return loss over the entire frequency band, the input impedance of cascade

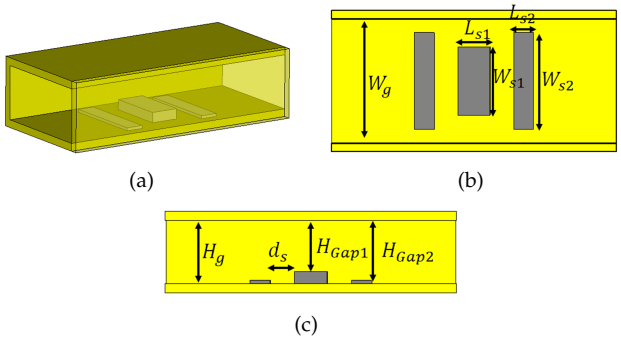


Fig. 5. The cascaded single ridge structure . (a) 3D cross-section view. (b) Side cross-section view. (c) Top cross-section view.

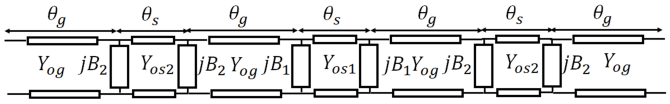


Fig. 6. The circuit model of cascaded single-ridge sections.

ridge structure is studied and plotted in Fig. 8. Due to the dispersive nature of each single-ridge structure, a significant variation of the real part of the overall input impedance is observed at the low frequency of the operating band. As shown in the analysis of the single-ridge characteristics impedance in equation 5, the TE mode causes a dispersive behaviour that is dependant on the cut-off frequency. To compensate for this behaviour, two cylindrical posts are added at both ends of the cascaded single ridges structure as shown in Fig. 9, to add two localized susceptances and provide a flatter response for the return loss curve. These posts are not only used for reducing the reflection imbalance, but also will allow a fine experimental tuning that compensates for the fabrication tolerances which are significant issue in mm-wave bands (such as the WR28 waveguide used in this paper). Fig. 10 shows the effect of the added posts on the reflection coefficient as a very flat return loss response is observed after adding these cylindrical posts.

Table I
THE DIMENSIONS OF THE MISMATCH SECTION IN INCHES

| RL | $L_{s1}$ | $L_{s2}$ | $W_{s1}$ | $W_{s2}$ | $H_{Gap1}$ | $H_{Gap2}$ | $d_s$ |
|---|---|---|---|---|---|---|---|
| 9.5 dB | 0.073 | 0.045 | 0.16 | 0.226 | 0.107 | 0.1325 | 0.061 |
| 12.7 dB | 0.073 | 0.045 | 0.155 | 0.22 | 0.1135 | 0.1325 | 0.057 |

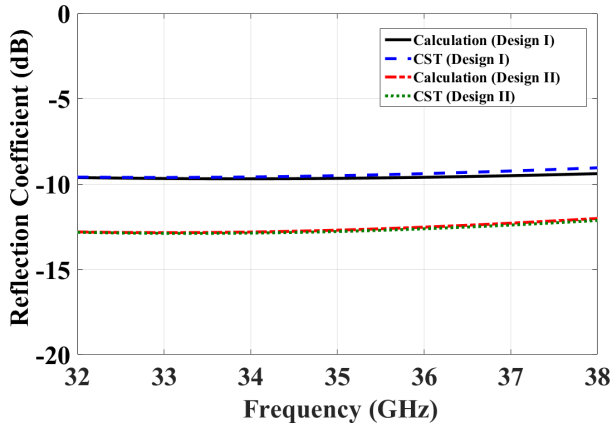


Fig. 7. Reflection coefficient for the cascaded single ridges structure.

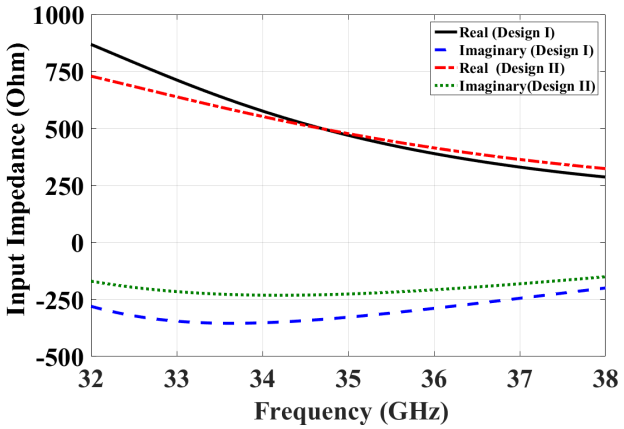


Fig. 8. The input impedance of the cascaded single ridges structure.

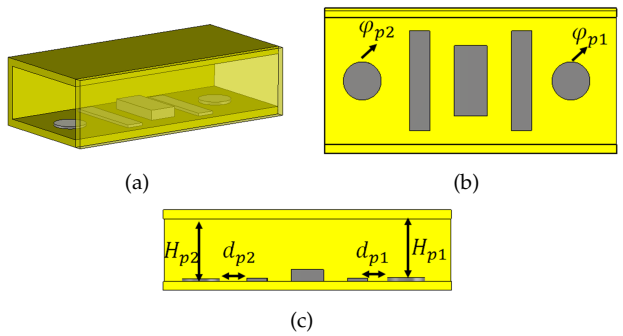


(a) (b)

(c)

Fig. 9. The cascaded single ridge structure with tuning post. (a) 3D cross-section view. (b) Side cross-section view. (c) Top cross-section view.

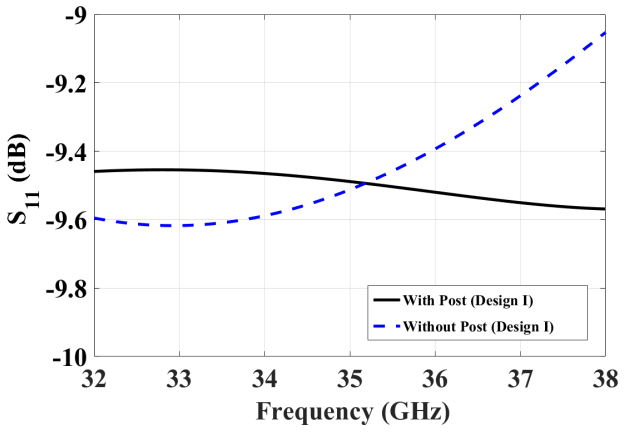


(a)

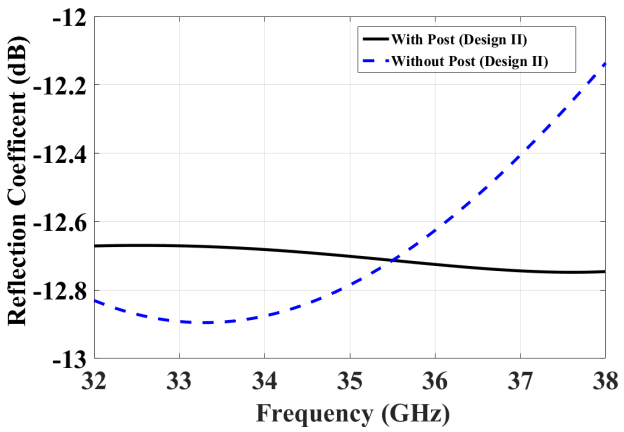


(b)

Fig. 10. Reflection coefficient for the cascaded single ridges structure with tuning post. (a) Design I. (b) Design II.

## IV. PRACTICAL CONSIDERATIONS

The proposed mismatch section is connected to a high power brick load. The load housing is fabricated using CNC machine with a tolerance of 0.0005" in all dimensions. The fabricated aluminum housing is made of two symmetric halves. The fabricated housing and the assembled mismatch load are shown in Figs. 11(a) and 11(b). Two different brick load units are used in this study. Several measurement are carried out for the two load units, where the average of the all measurement are calculated to overcome any calibration errors as shown in Fig. 12. It is shown that, the two load units have a different response. This means that, both units will have different response when connect the mismatch section. A comparison between the overall response of the measured mismatch termination using two different brick load units (Unit 1 and Unit 2) is shown in Fig.13. The measured response is for Design I (9.5 dB), and is carried out using Anritsu network analyzer. It is worth mentioning that, the simulation result is obtained assuming the brick load is deeply matched (assuming the line is terminated with $Z_o$). However, there is a significant discrepancy exists between the simulated and

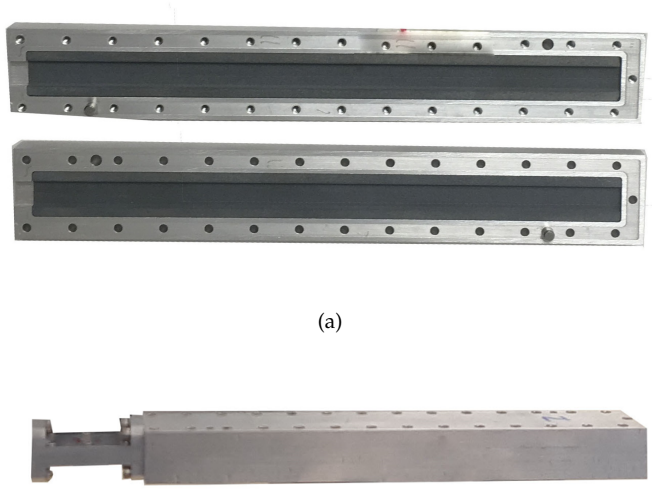

(a)

(b)

Fig. 11. Fabricated prototype of the mismatch load. (a) Brick load. (b) Assembled Mismatch load.

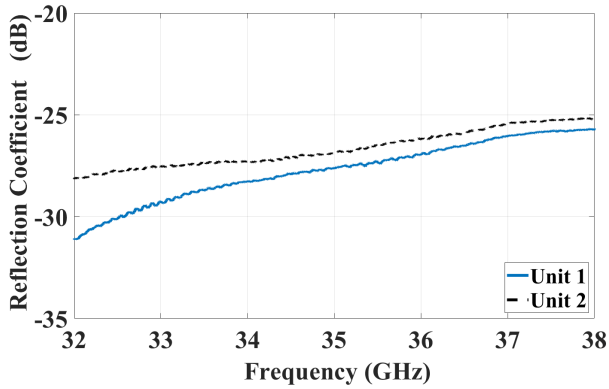


Fig. 12. The average reflection coefficient measurements of two different load units.

measured results. This can be explained by the realistic response of the high power brick load, while the design in the previous step assumed total signal absorption beyond the mismatch stage. Therefore, we would adapt our design procedure to take into account the limited matching level of the brick load, which not considered through the design process. This would dramatically affect the design, specially when the requirements of the mismatch section is relatively a low nominal reflection value such as the one used in this example. To take the brick load response into account, the dimensions of the mismatch section are re-optimized while the section in being loaded with the actual brick load measurements. The final response of the re-optimized dimensions will be addressed in the following section.

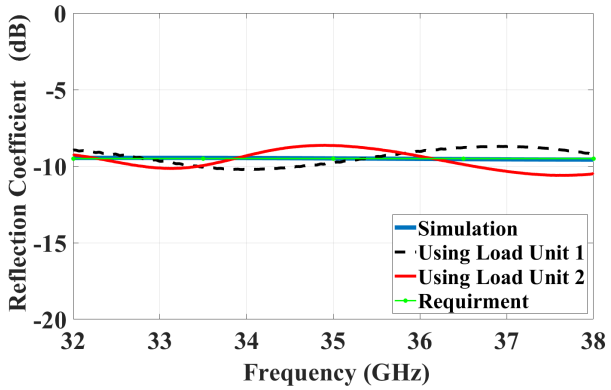


Fig. 13. Simulated with a perfect RF match load and measured reflection coefficient of the proposed design for 9.5 dB mismatch using a two different load units with brick load units 1 and 2.

## V. Experimental Results and Validation

The previously described design procedure is followed to propose a mismatch load design of reflection level 9.5dB. This unit is designed taking into account the measured response of the brick load (Unit 1) as indicated in the mentioned design procedure. The proposed final designs are fabricated and measured, where the measurement setup of these units are shown in Fig. 14(a). The measured response is compared with both the simulated and the model response in Figs. 14(b) and 14(c), where a good agreement is observed for both the reflection coefficient magnitude and phase, respectively. To evaluate the deviation of the measured results, the relative error of the measured reflection coefficient is shown in Fig. 15, where the error is below 10 % over the operating frequency band.

## VI. Conclusion

Mismatch loads are considered among the major components in multiple test setups for source evaluation and antenna response emulation. A straightforward and systematic procedure for the mismatch load is presented based on multiple single ridge sections surrounded by a cylindrical post at both ends. An accurate analytical model is proposed and validated for the single ridge sections, where a modified expression of the intermediate susceptance is proposed. Afterwards, the presented model is deployed to design two examples of mismatch sections. A significant contribution is introduced in this article through taking into account the actual brick load response in the design procedure. The fabricated designs based on the presented systematic procedure are measured, where the measured responses are in a good agreement with the simulated response.

## VII. Acknowledgment

The authors would like express their deepest appreciation for Scientific Microwave Corporation (SMC) team for their effort and support during the development of this article.

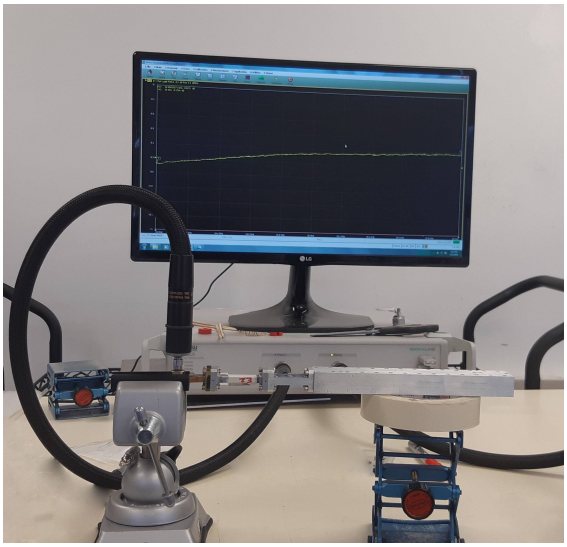

(a)

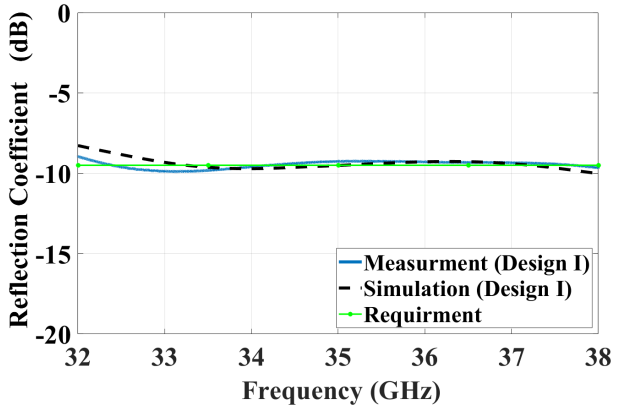


(b)

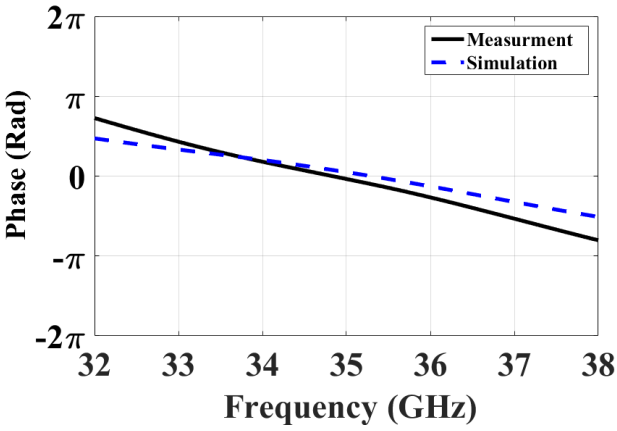


(c)

Fig. 14. (a) The test setup used for measurements. Simulated and measured RL for the 9.5 dB mismatch load considering the actual load measurements. (b) Magnitude. (c) Phase.

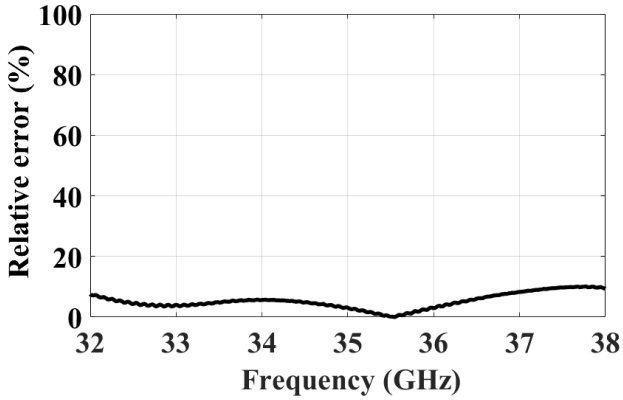


Fig. 15. The relative error between the measurement and simulation results.

## REFERENCES


[1] W. Hersch, "A very-wide-band dummy load for measuring power at very-high and ultra-high frequencies," Proc. Inst. Elect. Eng. B, vol. 102, no. 1, pp. 96-98, Jan., 1955.

[2] H. Matsumoto, Y. Iino, C. Fujiwara, Z. Kabeya, and T. Onda, "Experience on the high-power SiC microwave dummy-load using sic absorber," in Proc. IEEE Particle Accelerator Conf., vol. 2, pp. 842-844, Aug., 2002.

[3] J. Han, J.-H. Kim, S.-D. Park, M. Yoon, S. Y. Park, J. W. Shin, and J. H. So et al., "Coaxial-type water load for measuring high voltage, high current and short pulse of a compact Marx system for a high power microwave source," Phys. Rev. Special Topics-Accelerators Beams, vol. 12, no. 11, p. 113501, Nov., 2009.

[4] R. L. Ives, Y. M. Mizuhara, R. P. Pendleton, and R. V. Schumacher, "High Power Water Load for Microwave and Millimeter-Wave Radio Frequency Sources," U.S. Patent 5,949,298, Sep. 7, 1999.

[5] M. A. Panahi, S. Abdollah Ramezani, G. Ebrahimzadeh Ardakani and R. Safian, "An Efficient High Power RF Dummy-Load," in IEEE Microw. Wireless Compon. Lett., vol. 25, no. 6, pp. 409-411, Jun., 2015.

[6] V. Y. Kozhevnikov, A. I. Klimov and A. V. Kozyrev, "Simulation and optimization of dummy loads for microwave calorimeters," 22nd Telecommunications Forum Telfor (TELFOR), Belgrade, pp. 834-837, Feb., 2015.

[7] K. Ioki, S. Hiranai, S. Moriyama, and S. Tanaka, "Development of a dummy load and waveguide components for 1MW CW gyrotron", Fusion Engineering and Design, Vol. 109-111, Part A, pp. 951-955, Nov. 2016.

[8] C. Li, M. Zhang, K. X. Yu, X. Q. Qin, Z. Q. Song and P. Fu, "R&D on dummy load prototype for ITER coil power supply system,"26th IEEE Symposium on Fusion Engineering (SOFE), Austin, TX, pp. 1-5, Jun., 2016.

[9] Richard W. Brounley, P.E. "Mismatched Load Characterization for High-Power RF Amplifiers" High Frequency Electronics,pp. 30-38, Apr., 2004.

[10] C. Li, M. Zhang, K. X. Yu, X. Q. Qin, Z. Q. Song and P. Fu, "Dummy Load Prototype Design for ITER Coil Power Supply System," in IEEE Plasma Sci., vol. 44, no. 9, pp. 1711-1715, Sept. 2016.

[11] G. N. Kabdymanova, V. Y. Kozhevnikov, A. I. Klimov and A. V. Kozyrev, "Simulation of dummy load for L-S band high power microwave calorimeter," 2015 International Siberian Conference on Control and Communications (SIBCON), Omsk, pp. 1-4, Jul., 2015.

[12] X. Shen et al., "Decoupling of Two Strongly Coupled Dual-Band Antennas With Reactively Loaded Dummy Element Array," in IEEE Access, vol. 7, pp. 154672-154682, Oct., 2019,

[13] C. Zhang, Y. Jiao, J. Wen and Z. Weng, "Decoupling of Two Dual-Band Antennas With a Reactively Loaded Dummy Element," The International Symposium on Antennas and Propagation (ISAP), Xi'an, China, pp. 1-2, Jan. 2019.

[14] J.Helszajn,Ridge Waveguides and Passive Microwave Components, IEE electromagnetic waves series,Institution of Engineering and Technology,2000.
[15] Young, F., Hohmank, J. Characteristics of ridge waveguides. Appl. sci. Res. 8, 321-336 (1960).
[16] Yu Rong and K. A. Zaki, “Characteristics of generalized rectangular and circular ridge waveguides," in IEEE Trans. Microw. Theory Techn., vol. 48, no. 2, pp. 258-265, Feb., 2000.
[17] D. M. Pozar, Microwave Engineering, Hoboken, NJ, USA:Wiley, 2011.
[18] W. J. R. Hoefer and M. N. Burton, "Closed-Form Expressions for the Parameters of Finned and Ridged Waveguides," in IEEE Trans. Microw. Theory Techn., vol. 30, no. 12, pp. 2190-2194, Dec., 1982.
[19] S. B. Cohn, “Properties of ridge wave guide," Proc. IRE, vol. 35, no. 8, pp. 783-788, Aug. 1947.
[20] Y. Huang, N. Yang, S. Lin and R. F. Harrington, “Analysis of a post with arbitrary cross-section and height in a rectangular waveguide," in IEE P-MICROW. ANTEN. P., vol. 138, no. 5, pp. 475-480, Oct. 1991.
[21] A. G. Williamson, "Variable-length cylindrical post in a rectangular waveguide," in IEE P-MICROW ANTEN P., vol. 133, no. 1, pp. 1-9, Feb., 1986.
[22] N. Marcuvitz, "Waveguide Handbook," IEE electromagnetic waves series, McGraw-Hill,1951.
[23] J. Roelvink and A. G. Williamson, "Analysis of a solid variable-length cylindrical post in a rectangular waveguide," in IET Microw. Antennas Propag., vol. 1, no. 2, pp. 506-512, Apr., 2007.

**Shoukry I. Shams** (M’04) received the B.Sc. (with distinction) and M.Sc. degrees in electronics and communications engineering from Cairo University, Egypt, in 2004 and 2009, respectively. He received the PhD degree in electrical and computer engineering from Concordia University, Montréal, Québec, Canada in 2016. From 2005 to 2006, he served as a teaching and research assistant in the Department of Electronics and Communications Engineering, Cairo University. From 2006 to 2012, he served as a teaching and research assistant in the IET Department German University in Cairo. From 2012 to 2016, he was a teaching and research assistant with Concordia University. His research interests include microwave reciprocal/nonreciprocal design and analysis, high power microwave subsystems, antenna design and material measurement. Dr. Shams was the GUC-IEEE student branch chair 2010-2012. He received the Faculty Certificate of Honor in 1999, The Distinction with Honor in 2004 from Cairo University. He received the Concordia University Recruitment Award in 2012 and Concordia University Accelerator Award in 2016.

**Mahmoud Elsaadany** (M’18) received the B.Sc. (Hons.) and M.Sc. degree in electrical engineering from Cairo University, Egypt, in 2006 and 2010, respectively, and the Ph.D. degree in electrical and computer engineering from Concordia University, Montrŕal, QC, Canada, in 2018. Currently, Dr. Elsaadany is a research professional with École de technologie supérieure (ETS), Université du Québec. He was a Researcher with Qatar University, Qatar, from 2008 to 2010. His current research interests include digital signal processing, optimization of microwave components, machine-type communication, and algorithms design for the 5G cellular networks.

**Tayeb A. Denidni** (M’98SM’04F’19) received M. Sc. and Ph.D. degrees in electrical engineering from Laval University, Quebec City, QC, Canada, in 1990 and 1994, respectively. From 1994 to 2000, he was a Professor with the engineering department, UniversitÃ© du Quebec in Rimouski (UQAR), Rimouski, QC, Canada, where he founded the Telecommunications laboratory. Since 2000, he has been with the Institut National de la Recherche Scientifique (INRS), University of Quebec, Montreal, QC, Canada. He founded the RF Laboratory, INRS- Energie, Materiaux et Telecommunications (INRS-EMT), Montreal. He has extensive experience in antenna design. He served as a Principal Investigator on many research projects sponsored by NSERC, FCI, and numerous industries. His current research areas of interest include reconfigurable antennas using electromagnetic bandgap and frequency-selective surface structures, dielectric resonator antennas, meta- material antennas, adaptive arrays, switched multi-beam antenna arrays, ultrawideband antennas, microwave, and development for wireless communications systems.

**Mohamed Mamdouh M. Ali** (S’15) received the B.Sc. (with distinction) and M.Sc. degrees in electronics and communications engineering from Assiut University, Egypt, in 2010 and 2013, respectively. He received the PhD degree in electrical and computer engineering from Concordia University, Montréal, Québec, Canada in 2020. From 2010 to 2015, he was a Teaching and Research Assistant with the Department of Electronics and Communications Engineering, Assiut University. He was a Teaching and Research Assistant with Concordia University. His current research interests include microwave reciprocal/nonreciprocal and antenna design.

**Ghyslain Gagnon** received the Ph.D. degree in electrical engineering from Carleton University, Canada in 2008. He is now Dean of research and Professor at École de technologie supérieure, Montreal, Canada. He is a board member of ReSMiQ and was Director of research laboratory LACIME (2013-2020), a group of 15 faculties and nearly 150 highly dedicated students and researchers in microelectronics, digital signal processing and wireless communications. Highly inclined towards research partnerships with industry, his research aims at microelectronics, digital signal processing and machine learning with various applications, including health care, media art and building energy management.